Orbital-selective Mott phases of a one-dimensional three-orbital Hubbard model studied using computational techniques

Guangkun Liu, Nitin Kaushal, Shaozhi Li, Christopher B. Bishop, Yan Wang, Steve Johnston, Gonzalo Alvarez, Adriana Moreo, and Elbio Dagotto

Phys. Rev. E **93**, 063313 — Published 24 June 2016

DOI: 10.1103/PhysRevE.93.063313

Study of the Orbital-Selective Mott Phases of a One-Dimensional Three-Orbital Hubbard Model Using Computational Techniques

Guangkun Liu,[1,2] Nitin Kaushal,[1,3] Shaozhi Li,[1] Christopher B. Bishop,[1,3] Yan Wang,[1] Steve Johnston,[1] Gonzalo Alvarez,[4,5] Adriana Moreo,[1,3] and Elbio Dagotto[1,3]

[1] *Department of Physics and Astronomy, The University of Tennessee, Knoxville, Tennessee 37996, USA*
[2] *Department of Physics, Beijing Normal University, Beijing 100875, China*
[3] *Materials Science and Technology Division, Oak Ridge National Laboratory, Oak Ridge, Tennessee 37831, USA*
[4] *Center for Nanophase Materials Sciences, Oak Ridge National Laboratory, Oak Ridge, Tennessee 37831, USA*
[5] *Computer Science and Mathematics Division, Oak Ridge National Laboratory, Oak Ridge, Tennessee 37831, USA*

A recently introduced one-dimensional three-orbital Hubbard model displays orbital-selective Mott phases with exotic spin arrangements such as spin block states [J. Rincón *et al.*, Phys. Rev. Lett. **112**, 106405 (2014)]. In this publication we show that the Constrained-Path Quantum Monte Carlo (CPQMC) technique can accurately reproduce the phase diagram of this multiorbital one-dimensional model, paving the way to future CPQMC studies in systems with more challenging geometries, such as ladders and planes. The success of this approach relies on using the Hartree-Fock technique to prepare the trial states needed in CPQMC. We also study a simplified version of the model where the pair-hopping term is neglected and the Hund coupling is restricted to its Ising component. The corresponding phase diagrams are shown to be only mildly affected by the absence of these technically difficult-to-implement terms. This is confirmed by additional Density Matrix Renormalization Group and Determinant Quantum Monte Carlo calculations carried out for the same simplified model, with the latter displaying only mild Fermion sign problems. We conclude that these methods are able to capture quantitatively the rich physics of the several orbital-selective Mott phases (OSMP) displayed by this model, thus enabling computational studies of the OSMP regime in higher dimensions, beyond static or dynamic mean field approximations.

PACS numbers: 02.70.Ss, 71.30.+h, 71.27.+a, 71.10.Fd

I. INTRODUCTION

The study of iron-based high critical temperature superconductors continues attracting the attention of the condensed matter community [1–6]. Originally these materials were widely perceived as being in the weakly correlated regime, where Fermi surface nesting effects dominate; however, in recent times evidence has begun to accumulate indicating that the effects of electronic correlations cannot be neglected. This is manifested by substantial bandwidth reductions, the detection of localized spins at room temperature, and by the presence of superconductivity in cases with only electron pockets at the Fermi surface [3–5]. For these reasons, and since the iron pnictides and chalcogenides have several active $3d$ orbitals, it is very important to study multiorbital Hubbard models at intermediate Hubbard couplings U using reliable unbiased many-body techniques. There is, however, a notorious lack of appropriate computational methodologies for these demanding studies. In fact, the analysis of multiorbital Hubbard models at arbitrary couplings and temperatures is developing into a grand challenge for theoretical/computational physics.

In this publication, we present a systematic investigation of the properties of a recently introduced one-dimensional three-orbital Hubbard model [7, 8], using multiple techniques including Constrained-Path Quantum Monte Carlo (CPQMC), Determinant Quantum Monte Carlo (DQMC), and Density Matrix Renormalization Group (DMRG). Our conclusion is that CPQMC, when applied in the systematic manner described here, reproduces well the previously published DMRG results. As a consequence, CPQMC can address problems in higher dimensions, since this approach is not affected by the sign problem. We also have observed that a simplified Hubbard model, where the pair-hopping term has been discarded and the Hund interaction is reduced to its Ising component, leads to phase diagrams that are very similar to those of the full model. This simplification improves the performance of DQMC and other quantum Monte Carlo methods, since it alleviates the sign problem.

Our main focus is on the so-called Orbital-Selective Mott Phase (OSMP), a state widely discussed in multiorbital systems [9–19]. To focus on this state, our study will be mainly in the regime of robust Hund coupling strength that is compatible with a variety of investigations for iron-based superconductors [20–23]. In the OSMP, the occupation of one or more of the orbitals locks to one electron per orbital with increasing U/W (U is the on-site Hubbard repulsion and W is the electronic bandwidth), while the remaining orbitals have a fractional filling. For these reasons, this state has an intriguing combination of spin localized and charge itinerant degrees of freedom, as shown in several experiments on the iron based superconductors [3, 4, 25, 26]. Since the OSMP is also of potential value in several other correlated multiorbital systems, our investigations are of relevance beyond the realm of the iron-based superconductors.

The importance and richness of the OSMP regime is exemplified by the recent discovery of block states in pre-

vious DMRG studies of the one-dimensional three-orbital Hubbard model [7, 8]. Block states are formed by a small number of spins (the "block") that align ferromagnetically within the block, and with an antiferromagnetic coupling between blocks. These states have been reported in experimental and theoretical studies of two-leg ladder selenides belonging to the iron superconductors family [27–29], and it is intriguing to speculate on their possible existence in higher dimensional systems [30–32]. Moreover, recent investigations [8] unveiled the presence of three types of OSMP regimes, each differing with respect to the number of orbitals occupied by an integer number of electrons. These three OSMP phases are classified as follows: OSMP1 is the most canonical one, where one orbital's filling is locked to one electron per orbital, while the remaining two orbitals have fractional populations; OSMP2 appears for total electronic densities n between 3 and 4, and has two orbitals whose occupations are locked to one electron each, while the third orbital has a fractional filling; finally, OSMP3 was found for total fillings n between 4 and 5, and has one orbital locked with one electron, a second orbital locked with two electrons, and the third orbital has a fractional filling. For completeness, at small J/U (J is the strength of the Hund's coupling), a band insulator (BI) phase was also reported [7], with two orbitals doubly occupied and one orbital empty. A related BI and metallic phase (BI+M) also occurs, where two orbitals are close to being doubly occupied and the other one is almost empty. It is important to make sure whether these phases can be reached by CPQMC and DQMC as well.

The organization of this publication is as follows: the two models are defined in Sec. II and the technical details of our computational methods, particularly CPQMC and DQMC, are described in Sec. III. Section IV contains our main results, and finally in Sec. V we provide further discussion and present our conclusions.

II. MODEL

As already explained, we will focus on the one-dimensional three-orbital Hubbard model previously proposed and studied with the DMRG technique in Refs. 7 and 8. This model displays a robust OSMP regime in the phase diagram and hence it resembles qualitatively the physics expected to develop in realistic multiorbital models for the iron-based superconductors and related systems. In addition, the use of models that were previously analyzed computationally facilitates the comparison between our results and previous literature.

The model is composed of tight-binding and Coulombic interaction (restricted to be on site) terms: $H = H_{\rm t} + H_{\rm Coul}$. The tight-binding component is

$$H_{\rm t} = -\sum_{\mathbf{i}\sigma\gamma\gamma'} t_{\gamma\gamma'}(c^{\dagger}_{\mathbf{i}\sigma\gamma}c_{\mathbf{i}+1\sigma\gamma'} + \text{h.c.}) + \sum_{\mathbf{i}\sigma\gamma}\Delta_{\gamma}n_{\mathbf{i}\sigma\gamma}, \quad (1)$$

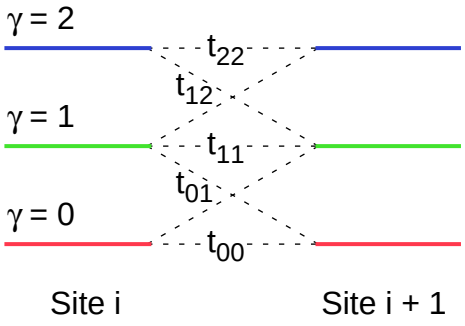

FIG. 1. (color online) Illustration of the hopping parameters of the one-dimensional three-orbital Hubbard model employed in this publication. Colored thick lines represent the orbitals γ (with $\gamma = 0, 1, 2$) at two lattice sites i and $i+1$, and the dashed black lines are the hoppings. Here t_{00}, t_{11}, and t_{22} correspond to the intra-orbital nearest-neighbor hoppings, while t_{01} and t_{12} are the inter-orbital hoppings.

where the operator $c^{\dagger}_{\mathbf{i}\sigma\gamma}$ ($c_{\mathbf{i}\sigma\gamma}$) creates (annihilates) an electron with spin z-axis projection σ at orbital γ ($\gamma = 0, 1, 2$) on lattice site $\mathbf{i}$. The number operator is $n_{\mathbf{i}\sigma\gamma} = c^{\dagger}_{\mathbf{i}\sigma\gamma}c_{\mathbf{i}\sigma\gamma}$. The hopping amplitudes $t_{\gamma\gamma'}$ defined in orbital space connect the lattice sites $\mathbf{i}$ and $\mathbf{i}+1$, with the specific values (eV units) $t_{00} = t_{11} = -0.5$, $t_{22} = -0.15$, $t_{02} = t_{12} = 0.1$, and $t_{01} = 0$, as schematically illustrated in Fig. 1. The total bandwidth is $W = 4.9|t_{00}|$ [7]. The orbital-dependent crystal-field splitting is denoted by Δ_{γ}, where we set $\Delta_0 = -0.1$, $\Delta_1 = 0$, and $\Delta_2 = 0.8$, following Refs. 7 and 8. The band structure of this model roughly resembles that of iron-based superconductors because it has hole and electron pockets centered at wavevectors $q = 0$ and π, respectively.

The interacting portion of the Hamiltonian is given by the usual electronic multiorbital terms and is defined as

$$H_{\rm Coul} = U\sum_{\mathbf{i}\gamma} n_{\mathbf{i}\uparrow\gamma}n_{\mathbf{i}\downarrow\gamma} + (U' - J/2)\sum_{\mathbf{i}\gamma<\gamma'} n_{\mathbf{i}\gamma}n_{\mathbf{i}\gamma'} - 2J\sum_{\mathbf{i}\gamma<\gamma'}\mathbf{S}_{\mathbf{i}\gamma}\cdot\mathbf{S}_{\mathbf{i}\gamma'} + J\sum_{\mathbf{i}\gamma<\gamma'}\left(P^{+}_{\mathbf{i}\gamma}P_{\mathbf{i}\gamma'} + \text{h.c.}\right). \quad (2)$$

Here, $\mathbf{S}_{\mathbf{i}\gamma} = \frac{1}{2}\sum_{\alpha,\beta} c^{\dagger}_{\mathbf{i}\alpha\gamma}\boldsymbol{\sigma}_{\alpha\beta}c_{\mathbf{i}\beta\gamma}$ ($\boldsymbol{\sigma}$ represents the Pauli matrices) is the total spin operator at orbital γ on lattice site $\mathbf{i}$, $n_{\mathbf{i}\gamma}$ is the electronic density, and $P_{\mathbf{i}\gamma} = c_{\mathbf{i}\downarrow\gamma}c_{\mathbf{i}\uparrow\gamma}$. The first two terms in Eq. 2 describe the intra- and inter-orbital Coulomb repulsion on the same lattice site, respectively. The third term contains the Hund coupling that favors the ferromagnetic alignment of the spins in different orbitals of the same lattice site. The pair-hopping is the fourth term and its coupling strength is equal to J. Note that U' satisfies the constraint $U' = U - 2J$, due to the orbital rotational invariance [33].

The model defined by Eqs. (1) and (2) will be referred to as the "full" model in this publication. We have also studied a "simplified" model with the same hopping terms but neglecting the spin-flip portion of the Hund's interaction (i.e. only the Ising contribution was used) as well as the pair-hopping interaction in Eq. (2). In doing so, we analyze the extent to which these terms affect the phase diagrams of the full model. Limited influences would be important for the state-of-art computational techniques since these terms are often cumbersome to implement and, more importantly, it can pave the way to simulations under more realistic circumstances, such as on ladder or two-dimensional geometries.

The corresponding interactions of the simplified model are

$$H_{\rm Coul}^{\rm Simple} = U\sum_{\mathbf{i}\gamma} n_{\mathbf{i}\uparrow\gamma}n_{\mathbf{i}\downarrow\gamma} + (U'-J/2)\sum_{\mathbf{i}\gamma<\gamma'} n_{\mathbf{i}\gamma}n_{\mathbf{i}\gamma'} - 2J\sum_{\mathbf{i}\gamma<\gamma'} \mathrm{S}^{\rm z}_{\mathbf{i}\gamma}\mathrm{S}^{\rm z}_{\mathbf{i}\gamma'}, \quad (3)$$

where $\mathrm{S}^{\rm z}_{\mathbf{i}\gamma}$ is the z-component of the spin operator $\mathbf{S}_{\mathbf{i}\gamma}$.

III. METHODS

A. Computational Techniques

We studied the full and simplified models numerically by using three powerful techniques: DMRG [34–36], DQMC [37, 38], and CPQMC [39–43]. Each of these techniques has its strengths and weaknesses. DMRG is widely recognized as the best technique for quasi one-dimensional systems although it is difficult to apply in higher dimensions. DQMC can be extended to higher dimensions but it suffers the infamous Fermion sign problem, even in one dimension [44, 45]. Finally, CPQMC does not have sign problems and can be used in any dimension, but the results depend on the trial wave function in some cases, as explained below. Since the CPQMC method has not received as much attention as the other two approaches mentioned here, it will be tested more extensively in the present study [46].

We now proceed with several goals in mind. First, we will test the CPQMC method in various three-orbital Hubbard model settings. We simulated the one-dimensional systems employing open boundary conditions (OBC) to facilitate a comparison with DMRG, which is known to work better under these boundary conditions. (In principle the performance of CPQMC is not expected to degrade with periodic boundary conditions.) Second, we wish to explore the effect of pair-hopping and spin-flip interactions by comparing the full and simplified models. Third, we wish to examine the extent of the sign problem when DQMC is applied to the simplified model. Surprisingly, we found that the sign problem is present but relatively mild. Finally, small discrepancies among the three techniques, especially for DMRG and CPQMC methods, will be discussed.

Since we are not modifying the standard DMRG protocol, here we will only describe in detail the CPQMC methodology, and, very briefly, the DQMC method. For more details about CPQMC and its applications to other multiorbital Hubbard models, we refer the reader to Refs. 40, 42, and 43 and references therein.

With regards to DMRG, typically 300 states per block were kept in the iterations and up to 25 sweeps were performed during the finite-size algorithm evolution (in some cases up to 600 states were used and up to 37 sweeps were done). Truncation errors were of the order of $\mathcal{O}(10^{-15})$. For each point in the phase diagram shown below, DMRG was run in the subspaces with zero and maximum total z-axis spin projections, and their energies were contrasted to address possible ferromagnetism (we observed that the ground states are all in either one or the other of those two total z-axis spin projections subspaces). Typical DMRG simulation times vary with the coupling strength U and electron doping n. Considering for example the $L = 16$ system, it requires $2 \sim 12$ hours for one point in the phase diagram, using 24 processors and the MPI technique.

B. Details of the CPQMC method

The CPQMC method is a sign-problem-free auxiliary-field quantum Monte Carlo method, which projects out the ground state from a trial state by branching random walks in the Slater determinant space. A constrained-path approximation is needed in the CPQMC algorithm to prevent the sign problem [40, 41]. Applications of CPQMC on various models and geometries yielded accurate results [40–43, 47–51].

In the CPQMC method, the ground state $|\Psi_{\rm g}\rangle$ is obtained by iteratively applying the projector operator $\mathrm{e}^{-\Delta\tau\hat{H}}$ to a trial state $|\Psi_{\rm T}\rangle$, with $\langle\Psi_{\rm g}|\Psi_{\rm T}\rangle \neq 0$. In order to implement the Monte Carlo steps, the projector $\mathrm{e}^{-\Delta\tau\hat{H}}$ is transformed into a summation of one-body operators, $\mathrm{e}^{-\Delta\tau\hat{H}} = \sum_{\{x\}} P(\{x\})\hat{B}(\{x\})$, by using the Hubbard-Stratonovich (HS) transformation [53] and Suzuki-Trotter decomposition. Here, $\{x\}$ is a set of Ising-like auxiliary fields introduced in the HS transformation, which can be interpreted as random variables distributed according to the probability distribution function $P(\{x\})$, while $\hat{B}(\{x\})$ is an $\{x\}$-dependent one-body operator. The procedure to transform the most complicated interactions, such as the Hund's coupling and pair-hopping terms, into one-body operators can be found in the Appendix [42, 54]. The Monte Carlo sampling of the set $\{x\}$ can be carried out according to $P(\{x\})$, propagating the wave-function, written as a Slater determinant $|\phi^{(m)}\rangle$, to a new one $|\phi^{(m+1)}\rangle$ via $|\phi^{(m+1)}\rangle = \hat{B}(\{x\})|\phi^{(m)}\rangle$, with $|\phi^{(0)}\rangle = |\Psi_{\rm T}\rangle$. The procedure, $|\phi^{(m)}\rangle \to |\phi^{(m+1)}\rangle$, is usually regarded as open-

ended branching random walks in the Slater determinant space.

In general, thousands of random walkers are employed in the CPQMC simulation. Because of the linearity of the Schrödinger equation, the random walks will naturally produce two sets of degenerate and mutually-canceling solutions, $\{|\phi\rangle\}$ and $\{-|\phi\rangle\}$. As a linear combination of $\{|\phi\rangle\}$ and $\{-|\phi\rangle\}$, the calculated ground state is basically dominated by the Monte Carlo noise. To control this problem, the random walks are constrained in CPQMC such that the condition $\langle\Psi_{\rm T}|\phi\rangle > 0$, which is also called the constrained-path approximation [40], is fulfilled at each Monte Carlo step.

After the random walks have equilibrated, expectation values can be estimated from the calculated ground state $|\Psi_{\rm C}\rangle$, which is a linear combination of random walkers with different weight factors. In principle, any observable $\mathcal{O}$ could be evaluated by using

$$\langle\mathcal{O}\rangle = \frac{\langle\Psi_{\rm C}|\mathcal{O}|\Psi_{\rm C}\rangle}{\langle\Psi_{\rm C}|\Psi_{\rm C}\rangle}. \tag{4}$$

However, such a "brute-force" way usually induces large fluctuations because in such a procedure $\langle\mathcal{O}\rangle$ contains many overlapping terms among different walkers, where each walker was propagated independently and without any knowledge of others. It is hard to reduce the statistical error by increasing the number of walkers N, since the error scales as $N^{-1/2}$. For observables $\mathcal{O}$ that commute with the Hamiltonian $\hat{H}$, an easy to implement and time-saving mixed estimator,

$$\langle\mathcal{O}\rangle_{\rm mixed} = \frac{\langle\Psi_{\rm T}|\mathcal{O}|\Psi_{\rm C}\rangle}{\langle\Psi_{\rm T}|\Psi_{\rm C}\rangle}, \tag{5}$$

usually gives high accuracy results. One can simply prove the accuracy of mixed estimator as follows,

$$\begin{aligned}\langle\mathcal{O}\rangle &= \frac{\langle\Psi_{\rm C}|\mathcal{O}|\Psi_{\rm C}\rangle}{\langle\Psi_{\rm C}|\Psi_{\rm C}\rangle} \\ &= \frac{\langle\Psi_{\rm T}|e^{-\beta\hat{H}}\mathcal{O}e^{-\beta\hat{H}}|\Psi_{\rm T}\rangle}{\langle\Psi_{\rm T}|e^{-2\beta\hat{H}}|\Psi_{\rm T}\rangle} \\ &= \frac{\langle\Psi_{\rm T}|\mathcal{O}e^{-2\beta\hat{H}}|\Psi_{\rm T}\rangle}{\langle\Psi_{\rm T}|e^{-2\beta\hat{H}}|\Psi_{\rm T}\rangle} = \langle\mathcal{O}\rangle_{\rm mixed},\end{aligned} \tag{6}$$

where $|\Psi_{\rm C}\rangle = e^{-\beta\hat{H}}|\Psi_{\rm T}\rangle = e^{-2\beta\hat{H}}|\Psi_{\rm T}\rangle$ when β is large. Because all the walkers originated from the initial state $|\Psi_{\rm T}\rangle$, mixed estimators have very small fluctuations.

For the observables $\mathcal{O}$ that do not commute with $\hat{H}$, it is sometimes possible to improve the mixed estimator by a linear extrapolation [39],

$$\langle\mathcal{O}\rangle_{\rm extr} = 2\langle\mathcal{O}\rangle_{\rm mixed} - \frac{\langle\Psi_{\rm T}|\mathcal{O}|\Psi_{\rm T}\rangle}{\langle\Psi_{\rm T}|\Psi_{\rm T}\rangle}. \tag{7}$$

Another widely used estimator involves the back-propagation (BP) [40]

$$\langle\mathcal{O}\rangle_{\rm BP} = \frac{\langle\Psi_{\rm T}|e^{-l\Delta\tau\hat{H}}\mathcal{O}|\Psi_{\rm C}\rangle}{\langle\Psi_{\rm T}|e^{-l\Delta\tau\hat{H}}|\Psi_{\rm C}\rangle}, \tag{8}$$

where l is typically in the range of 20 to 40. BP provides accurate estimates of ground-state properties in the Hubbard model [40, 41], and also shows a high degree of accuracy for the simplified model in our simulations. For the full model, however, our calculations suggest that BP can only work for a limited parameter regime, say $U/W < 0.25$; beyond this parameter regime BP always produces unacceptably large statistical errors. To explore the whole phase diagram here, we used the extrapolation method in Eq. (7) to estimate observables that do not commute with $\hat{H}$ for the full model while BP was used for the simplified model. We tested the results of the BP and extrapolation methods on the simplified model, and both methods predicted the same physics, i.e. the calculated energies of BP and extrapolation schemes are consistent as shown in Fig. 2(a). For this reason, we believe the extrapolation results capture the correct physics in the full model.

Based on the above discussion, together with the analysis of our simulation data, we conclude that the quality of the CPQMC calculation may depend on the trial wave function $|\Psi_{\rm T}\rangle$ to a certain extent: the trial state $|\Psi_{\rm T}\rangle$ always plays an important role, both in the constrained-path approximation and in the observable estimate. In order to get more accurate results and faster convergence speed, our CPQMC simulations were divided into three steps:

1. use the Hartree-Fock (HF) technique to construct a set of trial states with different magnetic orders;

2. use each of these HF states to carry out a set of independent CPQMC simulations;

3. obtain the final ground state from the completed CPQMC calculations by selecting the state with the lowest energy [52].

Following this strategy, each data point shown below (corresponding to a specific set of parameters U, J, and n) requires dozens of CPQMC simulations. The underlying reason for such massive efforts is that, in our three-orbital CPQMC calculations, different trial states often converge to different solutions each lying very close to one another in energy. Figure 2 (b) exemplifies a typical situation we observed: states with different magnetic orders are reached after starting from very different trial states, but sometimes their energies are so close that the system could be characterized to display the incorrect magnetic order. This may be different from the CPQMC calculations in the single-orbital models where the simulations seem to be insensitive to the trial wave function [40, 47, 48].

In addition, we found that the system was hard to converge to the ferromagnetic (FM) phase in the CPQMC calculation if it was initially starting from the $S^{\rm z}_{\rm total} = 0$ sector. To properly study the FM candidate, apart from the simulations in $S^{\rm z}_{\rm total} = 0$, we also forced the system

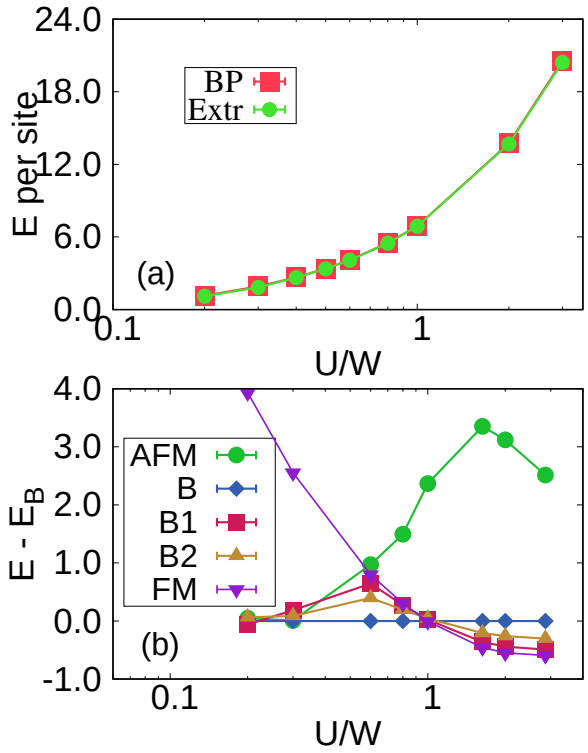

FIG. 2. (color online) (a) Results for the simplified model Eq. (3) using $L = 16$, $n = 4$, $J/U = 0.25$, and the CPQMC method. Shown is the energy per site obtained both by back propagation (BP) and by extrapolation (Extr) schemes. The agreement is clearly excellent. (b) The relative energies (with $|t_{00}| = 0.5$ as unit of reference) of the simplified model obtained from the CPQMC method. Results are shown for various trial states and reported with respect to the energy of the Block state with the spin configuration $\uparrow\uparrow\downarrow\downarrow$, at $n = 4$, $J/U = 0.25$, and using an $L = 16$ system. FM and AFM are ferromagnetic and staggered antiferromagnetic states, respectively. B, B2, and B1 represent the block states with the spin configurations $\uparrow\uparrow\downarrow\downarrow\uparrow\uparrow\downarrow\downarrow$, $\uparrow\uparrow\uparrow\uparrow\downarrow\downarrow\downarrow\downarrow$, and $\uparrow\uparrow\uparrow\uparrow\uparrow\uparrow\uparrow\uparrow\downarrow\downarrow\downarrow\downarrow\downarrow\downarrow\downarrow\downarrow$, respectively.

to start from the highest-S^{z}_{total} at a given filling. For instance, for two-thirds total filling (on average four electrons per site) on an L-site system, we set the number of electrons with up- and down-spin to be $3L$ and L, respectively, when searching for possible FM phases.

In a typical large-scale CPQMC simulation, we set the average number of random walkers to be 4800 and the time step is fixed at $\Delta\tau = \frac{0.03}{2|t_{00}|}$. For each walker, 2000 Monte Carlo steps were sampled before measurements were performed, and 20 blocks of 480 Monte Carlo steps each were used to ensure statistical independence during the measurements. Closed-shell fillings were employed in the simulations. To judge the accuracy of the CPQMC method, we compared the CPQMC energies against those employing the Lanczos method on a small $L = 4$ system

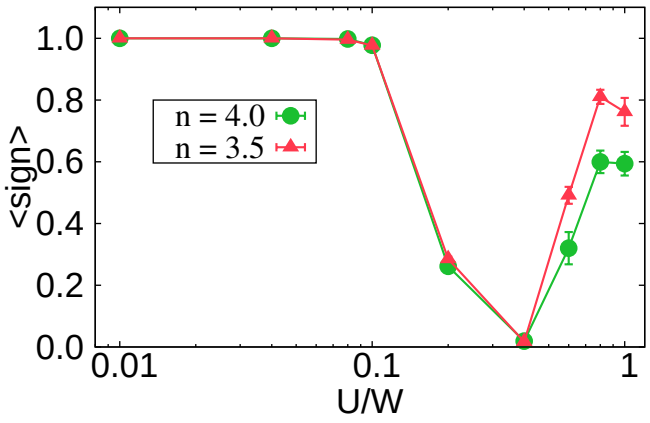

FIG. 3. (color online) DQMC results for the average value of the Fermion sign for the simplified model. Results are shown for average fillings $n = 3.5$ (red △) and 4.0 (green ◯), and at an inverse temperature of $\beta = 73.5/W$.

and also DMRG method on an $L = 16$ system: the maximum energy difference is within 1% up to $U/W = 3.0$.

Finally, note that because of the large computational time required for each set of parameters, MPI parallelism [55, 56] was integrated into the CPQMC algorithm. In the Monte Carlo procedure $|\phi^{(m)}\rangle \rightarrow |\phi^{(m+1)}\rangle$, each random walker $|\phi^{(m)}\rangle$ is independently propagated by $\hat{B}(\{x\})$. Therefore, it is natural to implement such a procedure in parallel by distributing the random walkers over multiple processors. The average observables for each processor were collected and averaged when necessary. This method was found to scale almost linearly. For instance, 4800 random walkers can be distributed evenly among 24 processors, and the computational time for one of these CPQMC simulations is approximately 2 hours. This can then be compared to the nearly 2 days of computational time when using only a single Intel Xeon E5-2680v3 core of the same type.

C. Details of the DQMC method and sign problem

DQMC is a numerically exact auxiliary-field method, capable of handling the Hubbard interactions non-perturbatively. The method [37, 38, 57], and its extension to multiorbital systems with inter-orbital density-density interactions relevant for this publication, can be found in Refs. 58 and 59. We refer the reader to these papers and references therein for further details.

The bottleneck of DQMC is the Fermion sign problem [45], which limits the range of accessible temperatures in many models. Generally speaking, severe Fermion sign problems would occur in the DQMC simulations of the multiorbital models with inter-orbital Hubbard and Hund's interactions and, worse, the severity of the problem increases when the off diagonal terms of the

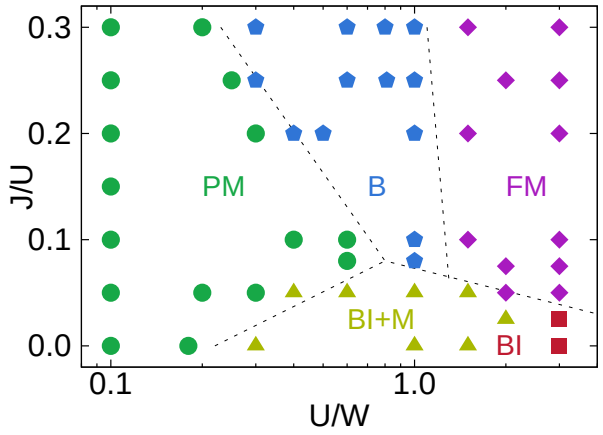

FIG. 4. (color online) The phase diagram of the full three-orbital Hubbard model Eq. (2) obtained using the CPQMC technique, employing chains with $L = 24$ sites and open boundary conditions. The electronic density is $n = 4$, and the notation for the many phases is explained in the text. Symbols indicate values of $(J/U, U/W)$ where explicit CPQMC results were obtained. Dashed lines are guides to the eye. This phase diagram is in good agreement with the DMRG results reported in Ref. 7 for the same model.

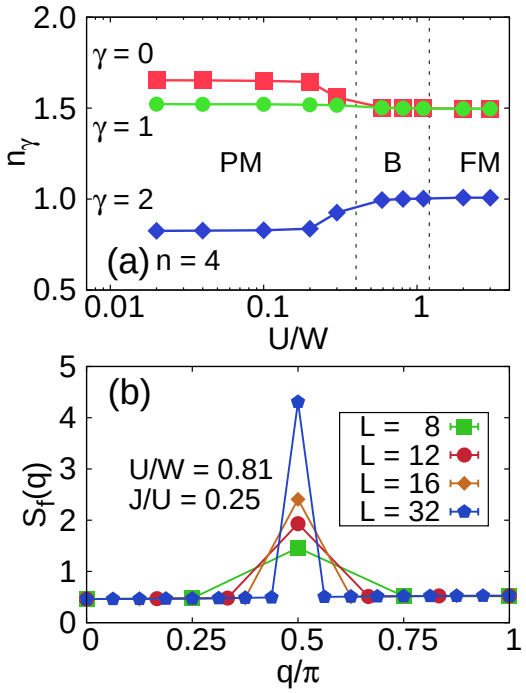

FIG. 5. (color online) CPQMC results for the full three-orbital model Eq. (2). (a) Electronic density n_γ of each orbital γ versus U/W at $n = 4$ and $J/U = 0.25$, using an $L = 24$ system with OBC; (b) Spin structure factor of the localized orbital $\gamma = 2$ in the OSMP Block regime at the couplings indicated, for several lattice sizes L and OBC.

interaction are included [54, 60, 61]. A recent study [44], however, has found that the sign problem in the single-band Hubbard model depends strongly on the geometry of the system. Similarly, it turns out that the simplified model [see Eq. (3)] has a manageable sign problem on the one dimensional lattice considered here. This is illustrated in Fig. 3, where we plot the average sign value as a function of U while holding $J = U/4$ fixed. Here, results are shown for an $L = 16$ chain and at an inverse temperature of $\beta = 73.5/W$, which is lower than temperatures that can be usually reached in the analogous two-dimensional model. One can see that the average value of the sign is quite high for most values of U, indicating that low temperature properties can be accessed. It is interesting to observe that the sign problem is at its worst when $U/W \sim 0.4$, which is near the phase boundary between the metallic and orbital-selective Mott phases for this model (see Sec. IV B).

IV. RESULTS

A. CPQMC results for the full Hubbard model

The phase diagram of the full model Eq. (2) obtained using the CPQMC method is presented in Fig. 4. The most striking result of this study is the clear resemblance of Fig. 4 with the phase diagram reported previously in Fig. 1 of Ref. 7 using the DMRG method. In particular, the paramagnetic metallic (PM) phase, the antiferromagnetic Block (B) phase, and the FM phase that dominate in the realistic Hund's coupling region $J/U \sim 0.25$ appear in very similar portions of the phase diagram. Also in excellent agreement with Ref. 7, the B and FM phases are in the OSMP regime as indicated by their relative orbital occupations, as shown in Fig. 5(a). In the B and FM phases, orbital 2 has $n_2 = 1$ while the population of the other two orbitals is non-integer for all values of U/W that we investigated. In Fig. 5(b) we show the magnetic structure factor in the localized band, defined as $S_f(\mathbf{q}) = 1/L \sum_{\mathbf{jm}} e^{i\mathbf{q}\cdot(\mathbf{j}-\mathbf{m})} \mathbf{S}_{\mathbf{j},\gamma=2} \cdot \mathbf{S}_{\mathbf{m},\gamma=2}$, which provides evidence for the "block" spin order ↑↑↓↓↑↑↓↓. Here, a sharp peak develops at wavevector $\pi/2$, similar to the results reported with DMRG [7]. In addition, the CPQMC method was also implemented using periodic boundary conditions and the Block phase was also found (our emphasis on OBC is for the comparison with DMRG). Also, the exotic low J/U region with a previously discussed BI and BI+M are found using both techniques. These results demonstrate that the most important aspects of the phase diagram are captured by CPQMC, not only qualitatively but also quantitatively in a one-dimensional system, suggesting that CPQMC can potentially be a reliable tool to study ladder and square lattice geometries for a wide parameter space that is difficult to address with other techniques.

There are two major differences between the CPQMC and DMRG results: First, CPQMC favors n_0 and n_1

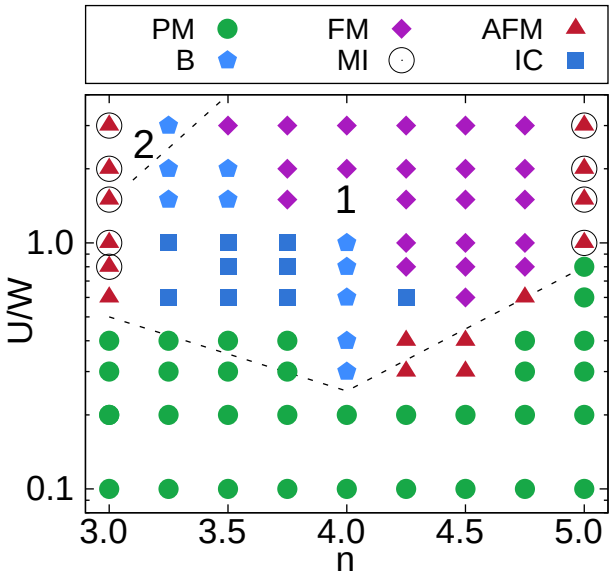

FIG. 6. (color online) The phase diagram of the full three-orbital model Eq. (2) obtained from CPQMC on an $L = 16$ system with OBC, and fixed $J/U = 0.25$. The meaning of the many symbols is explained in the top legend and in the main text. The numbers 1 and 2 in the figure represent the OSMP1 and OSMP2 phases, respectively, in the notation of Ref. 8. The dashed lines are guides to the eye. The notation B (block) encompasses different configurations: the block states at $n = 3.25$ and $n = 3.5$ are dominated by the spin configuration $\uparrow\uparrow\uparrow\uparrow\downarrow\downarrow\downarrow\downarrow$ and $\uparrow\uparrow\uparrow\uparrow\uparrow\uparrow\uparrow\uparrow\downarrow\downarrow\downarrow\downarrow\downarrow\downarrow\downarrow\downarrow$, while the block state at $n = 4$ contains the spin configuration $\uparrow\uparrow\downarrow\downarrow$.

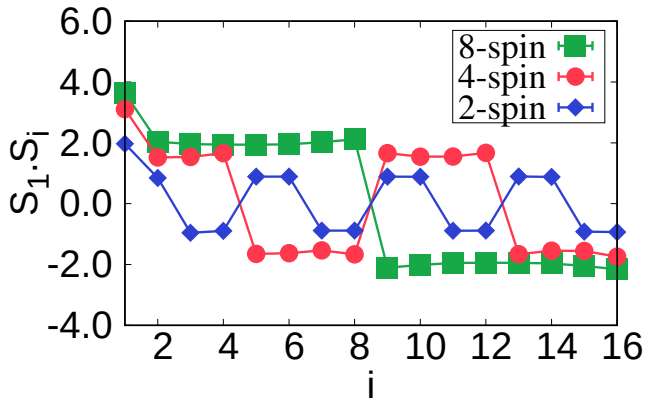

FIG. 7. (color online) Spin-spin correlations obtained using the CPQMC technique for the 2-spin block ($n = 4$, $U/W = 1.0$, $J/U = 0.25$), 4-spin block ($n = 3.5$, $U/W = 1.5$, $J/U = 0.25$) and 8-spin block ($n = 3.25$, $U/W = 2.0$, $J/U = 0.25$) states, using an $L = 16$ system and the full model.

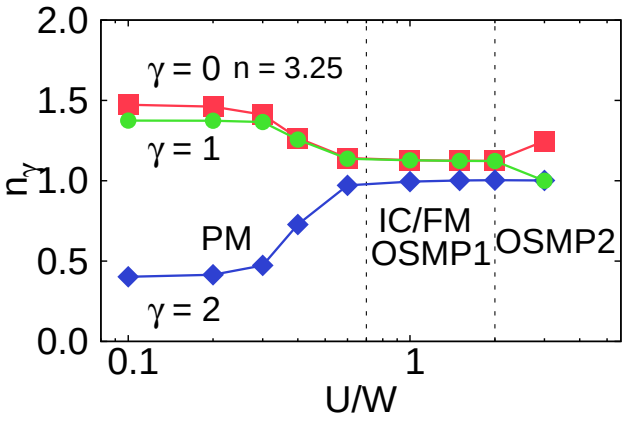

FIG. 8. (color online) CPQMC results for the full three-orbital model Eq. (2). The electronic density n_γ of each orbital γ versus U/W is shown for $n = 3.25$ and $J/U = 0.25$. The results were obtained using an $L = 16$ system with OBC. Phases OSMP1 and OSMP2 are defined in the text.

to be almost exactly 1.5 in the OSMP regime, while in the previous DMRG study those orbitals had populations close to but not precisely equal to 1.5. The consequences of this small difference remains to be studied; Second, we could not observe the Mott insulating regime with $n_1 = n_2 = 1$ and $n_0 = 2$ using the CPQMC method, which is stabilized in DMRG beyond $U/W \sim 4$. Since in CPQMC algorithm the HS fields were just flipped site-by-site, one possible reason for such a mismatch would be lacking of global flipping of the HS fields at large U/W, which is also a well-known problem in DQMC calculations [24]. Because the intermediate coupling region is the physically relevant region for the iron-based superconductors, this issue is not of immediate concern.

Let us focus now on the phase diagram varying the total electronic density $n = \frac{1}{L}\sum_{i\sigma\gamma} n_{i\sigma\gamma}$ at a fixed realistic $J/U = 0.25$, relevant for the iron-based superconductors. The CPQMC results are shown in Fig. 6, and they should be contrasted against the DMRG phase diagram presented in Fig. 1 of Ref. 8. Once again there are strong similarities, and the important PM, B (including incommensurate IC), and FM phases are present in both cases and in approximately similar regions of the phase diagram. This includes the realistic U/W regimes relevant for the iron superconductors. Note that the B phase regime not only includes the structure with wavevector $\pi/2$ mentioned before, but also more extended structures with larger FM blocks involving 4 and 8 sites, or directly involving incommensurate states. The real-space spin-spin correlations for several typical points in the B phase regime can be found in Fig. 7. In both phase diagrams, this generalized B phase regime is more robust upon hole doping ($n < 4$) away from the $n = 4$ state than upon electron doping ($n > 4$).

Evidence for the presence of an OSMP region using the CPQMC technique is provided in Fig. 8, where the OSMP1 notation is used for the OSMP phase found at $n = 4$ with only one orbital locked at one electron per orbital. These results for the individual orbital populations

vs. U/W are also very similar to those in Ref. 8.

Two additional discrepancies between the DMRG and CPQMC results are worth noting. First, as in the previous figures at $n = 4$, CPQMC has difficulty reaching very large values of U/W. For this reason, the so-called OSMP2 and OSMP3 phases reported in Ref. 8 have not been observed here (with the exception of one point at $n = 3.25$). OSMP2 is characterized by having two orbitals whose average occupation is locked to $n_\gamma = 1$, while OSMP3 has one orbital with $n = 1$ and another with $n = 2$. Second, a small region of antiferromagnetism with wavevector $q = \pi$ is found upon electron doping the $n = 4$ state in a region where DMRG suggests that only the PM, FM, and B phases should have similar energies. The CPQMC result is surprising and probably spurious, as there is no reason for a spin staggered state to be stabilized by doping.

To summarize this section, the CPQMC method has captured the most important aspects of the phase diagram of the full model Eq. (2) previously studied with DMRG. For this reason, CPQMC is a promising technique to study phase diagrams of multiorbital models in ladder or square lattice geometries, where DMRG faces a considerable challenge due to the fast growth of the required number of states and where DQMC has significant sign problems.

B. Results for the simplified Hubbard model

Our second goal is to test if the simplified version Eq. (3) of the full Hamiltonian, i.e. without the pair-hopping term and restricting the Hund interaction to its Ising component, leads to phase diagrams similar to those of the full model. If this were the case, this simplified model would be technically easier to study with computational methods than the full model.

1. *DMRG results*

Let us start with the U/W vs. n phase diagram at $J/U = 0.25$ obtained using DMRG. The results are shown in Fig. 9 and should be contrasted against those reported for the full model in Ref. 8, as well as with the CPQMC results in Fig. 4. The similarities in the phase diagrams produced by the full and simplified models is clear: the PM, Block/IC, FM, and AFM phases appear all approximately in the same locations in both models (note that, as expected, the absence of spin-flip terms in the Hund component reduces the critical U/W for magnetic order particularly at $n = 4$ and 5 when Fig. 9 is compared with the phase diagram of Ref. 8). These results suggest that the simplified model captures the same physics as the full model, with the advantage that it is technically easier to study.

This conclusion is also supported by the orbital occupations. Figure 10 illustrates the behavior of the electronic density vs. U/W at $J/U = 0.25$ at the representative electronic densities $n = 3.5, 4.0$, and 4.5. The presence of the OSMP1, OSMP2, and OSMP3 phases is clear.

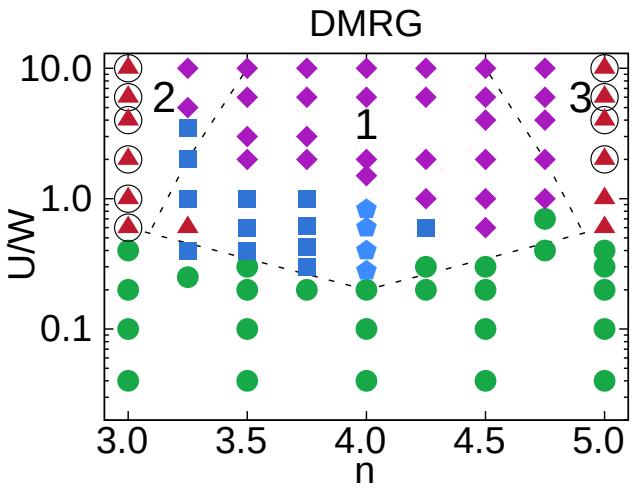

FIG. 9. (color online) DMRG results for the simplified three-orbital model Eq. (3). Shown is the phase diagram using an $L = 16$ system, OBC, and working at fixed $J/U = 0.25$. The many symbols were explained in the top caption of Fig. 6. The labels 1, 2, and 3 represent the OSMP1, OSMP2, and OSMP3 states in the notation of Ref. 8 (also explained in the text).

2. *DQMC results*

In principle, the DQMC technique applied to a multi-orbital Hubbard model can suffer from a severe sign problem, particularly when interorbital Hubbard and Hund's interactions are included. In addition, the HS decoupling of the complicated interactions characteristic of a multi-orbital Hubbard model, such as for example the pair-hopping term, significantly exacerbates the Fermion sign problem; however, when DQMC is implemented for the simplified model we have found that the sign problem is relatively mild in one dimension, and only particularly bad in the vicinity of one value of U/W (close to the PM-OSMP1 transition) as shown in Fig. 3. Thus, DQMC simulations are possible for this simplified model down to relatively low temperatures. Unfortunately, obtaining DQMC results is still computationally demanding even for this simplified case. Our study here is therefore restricted to selected values of n at $J/U = 0.25$ (note also that at the low temperatures of focus here the DQMC grand canonical ensemble results can be compared with the zero temperature CPQMC and DMRG canonical ensemble results).

In Fig. 11(a) DQMC results at $n = 4$ are shown, illustrating the presence of the OSMP1 phase. In addition, the spin structure factor arising from the localized orbital $\gamma = 2$ indicates a peak at wavevector $q = \frac{\pi}{2}$, in agree-

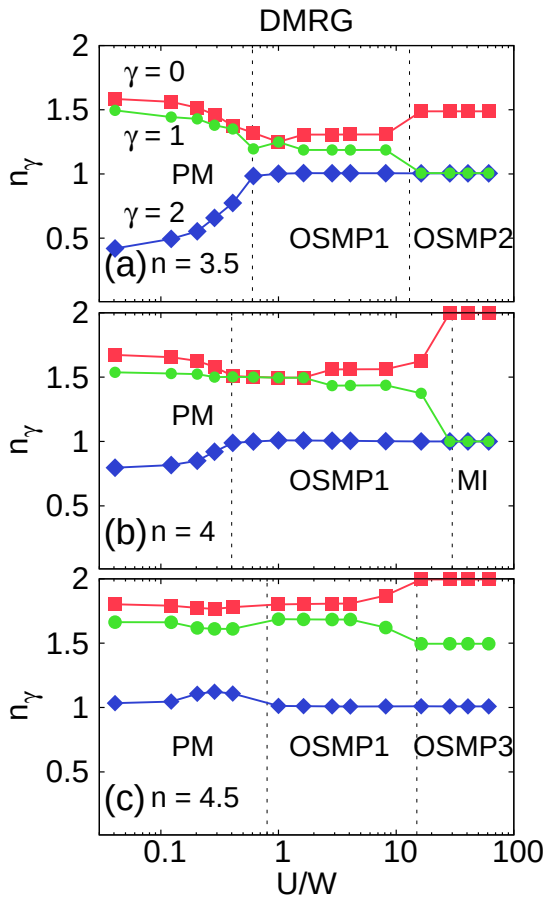

FIG. 10. (color online) DMRG results for the simplified three-orbital model Eq. (3), working at $J/U = 0.25$ and using an $L = 16$ system with OBC. Shown is the electronic density n_γ of each orbital γ versus U/W at (a) $n = 3.5$, (b) $n = 4.0$, and (c) $n = 4.5$.

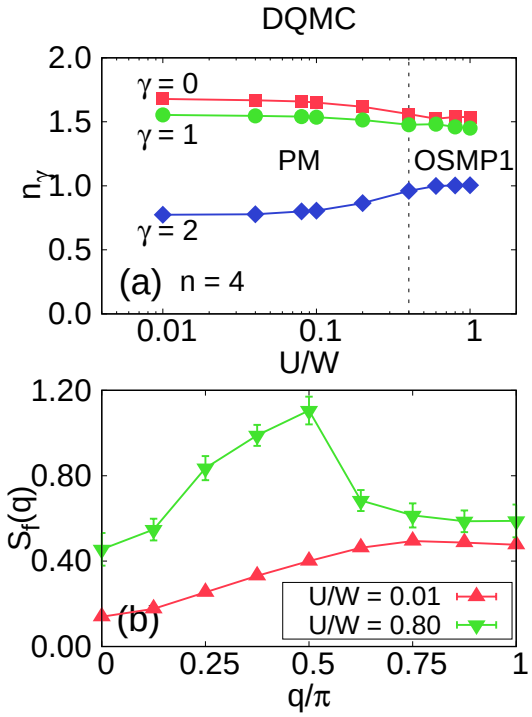

FIG. 11. (color online) DQMC results for the simplified three-orbital model Eq. (3) in the OSMP1 regime, using a chain with $L = 16$ sites and open boundary conditions. The temperature is $\beta = 73.5/W$. (a) Electronic density n_γ for each orbital γ versus U/W at $n = 4$ and $J/U = 0.25$. (b) Spin structure factor for the localized orbital $\gamma = 2$ at the values of U/W indicated and $J/U = 0.25$. The peak at $q = \frac{\pi}{2}$ denotes a tendency towards spin blocks with two aligned spins in each.

ment with the other techniques, and characteristic of the Block phase with FM blocks involving two spins. Similar results are obtained at $n = 3.5$, as shown in Fig. 12. In this case, the spin structure factor peaks at wavevector $q = \frac{3\pi}{4}$, also in agreement with the other techniques (although not strictly rigorous due to finite size effects, we refer to this type of magnetic spin states as incommensurate). Note that the spin structure factor is not so sharp due to the elevated temperature in the DQMC calculations. We also note that the locking of orbital occupancies was generally observed at much higher temperatures than where the onset of the magnetic correlations in $S_f(\mathbf{q})$ was investigated.

3. *CPQMC results*

To finalize our analysis of the simplified model, let us now examine the results obtained with the CPQMC method. The U/W vs. n phase diagram at $J/U = 0.25$ is presented in Fig. 13. The agreement with the DMRG phase diagram Fig. 9 and with the DMRG results of Ref. 8 is excellent showing once again that this method is promising and could work in higher dimensions as well. Note that the (likely spurious) antiferromagnetic phase centered at $n = 4.5$ at the frontier with the PM regime is no longer present in this simplified model.

Finally, Fig. 14 indicates that CPQMC can capture the physics of the three-orbital selective Mott states of relevance, i.e. OSMP1, OSMP2, and OSMP3.

V. DISCUSSION AND CONCLUSIONS

We have studied a three-orbital Hubbard model defined in one dimension using three powerful many-body computational techniques: CPQMC, DMRG, and DQMC. The specifics of the model, and in particular its hopping amplitudes, were chosen to match those of a previous DMRG investigation [7] in order to have available results to judge the accuracy of the three methodologies employed here. Our investigations allow us to reach three concrete conclusions: *(i)* The CPQMC technique,

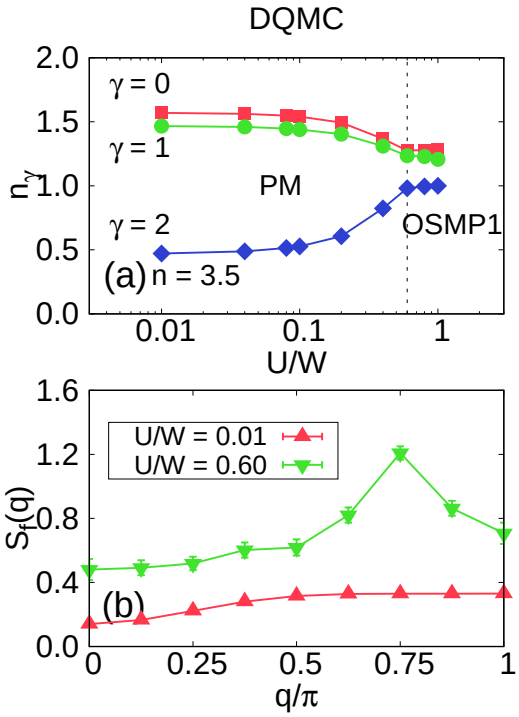

FIG. 12. (color online) DQMC results for the simplified three-orbital model Eq. (3) in the OSMP1 regime, using a chain with $L = 16$ sites and open boundary conditions. The temperature is $\beta = 73.5/W$. (a) Electronic density n_γ for each orbital γ versus U/W at $n = 3.5$ and $J/U = 0.25$. (b) Spin structure factor for the localized orbital $\gamma = 2$ at the value of U/W indicated and $J/U = 0.25$. The peak at $q = \frac{3\pi}{4}$ indicates a tendency towards spin incommensurate order.

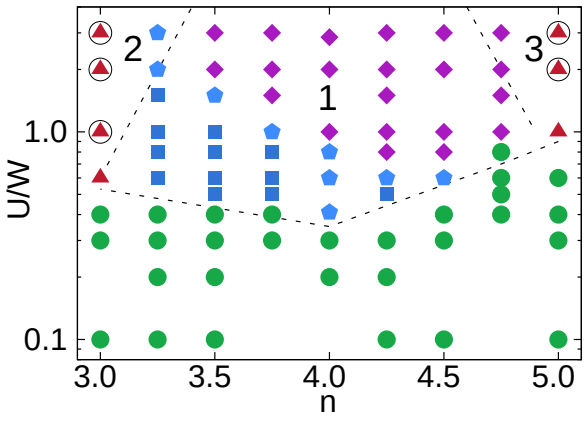

FIG. 13. (color online) CPQMC results for the simplified three-orbital model Eq. (3). Shown is the phase diagram using an $L = 16$ system, OBC, and working at fixed $J/U = 0.25$. The meaning of the many symbols is in the top caption of Fig. 6. The labels 1, 2, and 3 represent the OSMP1, OSMP2, and OSMP3 states in the notation of Ref. 8 (also explained in the text). The notation B (block) is generic, as explained in the text, and does not refer only to ferromagnetic blocks of just two spins. Dashed lines are guides to the eye.

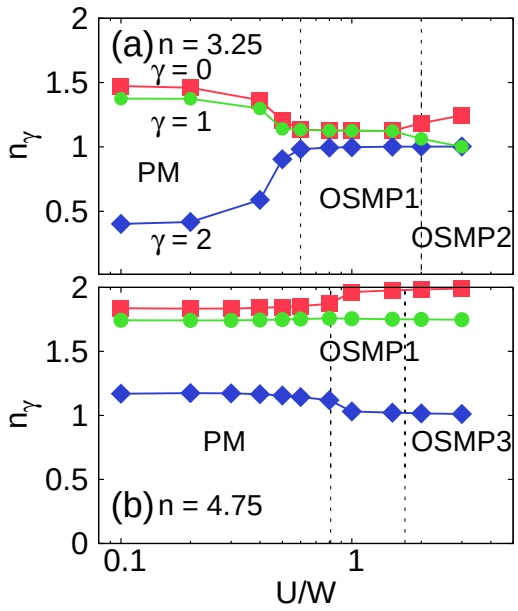

FIG. 14. (color online) CPQMC results for the simplified model Eq. (3), working at $J/U = 0.25$ and using an $L = 16$ system with OBC. Shown is the electronic density n_γ of each orbital γ vs. U/W at (a) $n = 3.25$ and (b) $n = 4.75$.

when applied as described in Sec. III, produces results in good agreement with the more powerful (in one dimension) DMRG method. This test paves the way for future CPQMC investigations in ladders or two dimensional systems, where DMRG or DQMC are difficult to apply; *(ii)* The simplified model defined here, without the pair-hopping term and keeping only the Ising term in the Hund interaction, captures quantitatively the phase diagrams of the full model, and in particular the important OSMP regime with its Block and FM phases. Thus, this simplified model can be used as an alternative to the full Hubbard model in future investigations; *(iii)* The DQMC technique works well for the simplified model since the sign problem is not severe in one dimension. While this conclusion will not hold in higher dimensions, we note that there are several strongly correlated electronic materials with quasi-one-dimensional dominant structures. Our results demonstrate that simplified multiorbital Hubbard models and DQMC methods can now be used to explore their properties at finite temperatures and interaction strengths U/W and J/U, thus opening a broad area of research.

In summary, our investigation paves the way toward computational studies of multiorbital Hubbard models in chains, ladders, and planes. The analysis of these models is a rapidly growing area of interest within strongly correlated electrons because of their importance in active fields such as iron-based high critical temperature superconductors, as well as in a variety of transition metals oxides such as manganites where previous work also unveiled a variety of competing states in their phase dia-

grams [33, 62–65].

VI. ACKNOWLEDGMENTS

G.L. thanks Shuhua Liang, Julián Rincón and Qinlong Luo for insightful discussions. G.L., N.K., C.B., A.M., and E.D. were supported by the National Science Foundation Grant No. DMR-1404375. G.L. was also supported by the China Scholarship Council. G.L., N.K., and C.B. are also partially supported by the U.S. Department of Energy (DOE), Office of Basic Energy Science (BES), Materials Science and Engineering Division. G.A. was supported by the Center for Nanophase Materials Sciences, sponsored by the U.S. Department of Energy (DOE), and the DOE early career research program. Y.W., S.L., and S.J. were supported by the University of Tennessee's Science Alliance Joint Directed Research and Development (JDRD) program, a collaboration with Oak Ridge National Laboratory. The DQMC calculations used computational resources supported by the University of Tennessee and Oak Ridge National Laboratory's Joint Institute for Computational Sciences and resources of the National Energy Research Scientific Computing Center (NERSC), a DOE Office of Science User Facility.

VII. APPENDIX

To decouple the Hund's coupling and pair hopping terms in Eq. (11) into practical forms, we rewrite the interaction portion of the full Hamiltonian as follows,

$$H_{\text{Coul}} = \textstyle\sum_{\mathbf{i}}(H_1^{\mathbf{i}} + H_2^{\mathbf{i}} + H_3^{\mathbf{i}} + H_4^{\mathbf{i}}), \tag{9}$$

$$H_1^{\mathbf{i}} = J\textstyle\sum_{\gamma\neq\gamma'}(c^\dagger_{\mathbf{i}\gamma\uparrow}c^\dagger_{\mathbf{i}\gamma'\downarrow}c_{\mathbf{i}\gamma\downarrow}c_{\mathbf{i}\gamma'\uparrow} + c^\dagger_{\mathbf{i}\gamma\uparrow}c^\dagger_{\mathbf{i}\gamma\downarrow}c_{\mathbf{i}\gamma'\downarrow}c_{\mathbf{i}\gamma'\uparrow}), \tag{10}$$

$$H_2^{\mathbf{i}} = (U'-J)\textstyle\sum_{\sigma,\gamma<\gamma'} n_{\mathbf{i},\prime,\sigma}n_{\mathbf{i},\gamma',\sigma}, \tag{11}$$

$$H_3^{\mathbf{i}} = U\textstyle\sum_{\gamma} n_{\mathbf{i}\gamma\uparrow}n_{\mathbf{i}\gamma\downarrow}, \tag{12}$$

$$H_4^{\mathbf{i}} = U'\textstyle\sum_{\sigma,\gamma<\gamma'} n_{\mathbf{i},\gamma,\sigma}n_{\mathbf{i},\gamma',-\sigma}, \tag{13}$$

where γ ($\gamma = 0, 1, 2$) denotes the orbitals. Note that $H_2^{\mathbf{i}}$, $H_3^{\mathbf{i}}$, and $H_4^{\mathbf{i}}$ can be decoupled by the standard discrete Hubbard-Stratonovich (HS) transformation [53]. However, $H_1^{\mathbf{i}}$ needs a special treatment [54] and it can be decoupled as,

$$e^{-\Delta\tau H_1^{\mathbf{i}}} = \frac{1}{2}\sum_{\alpha=\pm1} e^{\lambda\alpha(f_{\mathbf{i}\uparrow}-f_{\mathbf{i}\downarrow})}e^{a(N_{\mathbf{i}\uparrow}+N_{\mathbf{i}\downarrow})+bN_{\mathbf{i}\uparrow}N_{\mathbf{i}\downarrow}}, \tag{14}$$

with

$$f_{\mathbf{i},\sigma} = c^\dagger_{\mathbf{i},\gamma,\sigma}c_{\mathbf{i},\gamma',\sigma} + c^\dagger_{\mathbf{i},\gamma',\sigma}c_{\mathbf{i},\gamma,\sigma}, \tag{15}$$

$$N_{\mathbf{i},\sigma} = n_{\mathbf{i},\gamma,\sigma} + n_{\mathbf{i},\gamma',\sigma} - 2n_{\mathbf{i},\gamma,\sigma}n_{\mathbf{i},\gamma',\sigma}, \tag{16}$$

$$\lambda = \frac{1}{2}\log(e^{2J\Delta\tau} + \sqrt{e^{4J\Delta\tau}-1}), \tag{17}$$

$$a = -\log(\cosh(\lambda)), b = \log(\cosh(J\Delta\tau)), \tag{18}$$

where $\alpha = \pm1$ is the newly introduced auxiliary field, and γ continues denoting the different orbitals.

Due to the property that $N^2_{\mathbf{i},\sigma} = N_{\mathbf{i},\sigma}$, the factor $e^{bN_{\mathbf{i}\uparrow}N_{\mathbf{i}\downarrow}}$ in Eq. (14) can be further decoupled into a product of single $e^{N_{\mathbf{i}\sigma}}$-like terms using the discrete HS transformation [53].

The main challenge now will be how to treat the factor $e^{\lambda\alpha(f_{\mathbf{i}\uparrow}-f_{\mathbf{i}\downarrow})}$ in Eq. (14). Let us recall that in the standard QMC algorithm the matrix form of an exponential interaction term, such as the Hubbard repulsion $e^{H_3^{\mathbf{i}}}$ for example, always has the form

$$e^{H_3^{\mathbf{i}}} = I + A, \tag{19}$$

where A is a sparse matrix with and only with nonzero diagonal elements and I is the identity matrix. Because A only contains diagonal elements, the determinant division $\frac{\det\langle\phi'|e^{H_3^i}|\phi\rangle}{\det\langle\phi'|\phi\rangle}$ and the matrix inverse $(\langle\phi'|e^{H_3^i}|\phi\rangle)^{-1}$, which are necessary intermediate quantities used in the QMC algorithm, can be efficiently calculated using a fast updating tactic [38], while direct calculations of determinant and matrix inverse would be too time-consuming to use in QMC simulations ($|\phi\rangle$ represents the random walker).

The matrix form of $e^{\lambda\alpha f_{\mathbf{i}\sigma}} = e^{\lambda\alpha(c^\dagger_{\mathbf{i},\gamma\sigma}c_{\mathbf{i},\gamma'\sigma}+\text{h.c.})} = I+B$ is very different from the standard case shown in Eq. (19) because B contains two nonzero diagonal and another two non-diagonal elements:

$$B = \begin{pmatrix} \ddots & & & & \\ & b_{mm} & \cdots & b_{mn} & \\ & \vdots & \ddots & \vdots & \\ & b_{nm} & \cdots & b_{nn} & \\ & & & & \ddots \end{pmatrix}, \tag{20}$$

where $b_{mm} = b_{nn} = \frac{e^{-\lambda\alpha}+e^{\lambda\alpha}}{2} - 1$, $b_{mn} = b_{nm} = \frac{-e^{-\lambda\alpha}+e^{\lambda\alpha}}{2}$, and m, n refer to the matrix element indexes. To calculate the determinant division $\frac{\det\langle\phi'|e^{\lambda\alpha f_{\mathbf{i}\sigma}}|\phi\rangle}{\det\langle\phi'|\phi\rangle}$ and matrix inverse $(\langle\phi'|e^{\lambda\alpha f_{\mathbf{i}\sigma}}|\phi\rangle)^{-1}$ by using the fast updating algorithm [38], these formulas need further modifications. Consider the treatment of the determinant division for example. Here, we first insert two identity matrices $I = UU^{-1}$ into the determinant division, i.e. $\frac{\det\langle\phi'|UU^{-1}e^{\lambda\alpha f_{\mathbf{i}\sigma}}UU^{-1}|\phi\rangle}{\det\langle\phi'|\phi\rangle}$. The unitary matrix U always has the form

$$U = \begin{pmatrix} 1 & & \cdots & & 0 \\ & -\frac{\sqrt{2}}{2} & \cdots & \frac{\sqrt{2}}{2} & \\ \vdots & \vdots & \ddots & \vdots & \vdots \\ & \frac{\sqrt{2}}{2} & \cdots & \frac{\sqrt{2}}{2} & \\ 0 & & \cdots & & 1 \end{pmatrix}, \tag{21}$$

where we can find the expected four $\frac{\sqrt{2}}{2}$-related elements mentioned above, while all other diagonal and non-diagonal elements are just 1 and 0, respectively.

It can be easily proved that

$$\begin{aligned}\frac{\det\langle\phi'|e^{\lambda\alpha f_{i\sigma}}|\phi\rangle}{\det\langle\phi'|\phi\rangle} &= \frac{\det\langle\phi'|UU^{-1}e^{\lambda\alpha f_{i\sigma}}UU^{-1}|\phi\rangle}{\det\langle\phi'|\phi\rangle} \\ &= \frac{\det\langle\psi'|U^{-1}e^{\lambda\alpha f_{i\sigma}}U|\psi\rangle}{\det\langle\phi'|\phi\rangle} \\ &= \frac{\det\langle\psi'|(I+B')|\psi\rangle}{\det\langle\phi'|\phi\rangle},\end{aligned} \tag{22}$$

where $\langle\psi'| = \langle\phi'|U$, $|\psi'\rangle = U^{-1}|\phi\rangle$. And $U^{-1}e^{\lambda\alpha f_{i\sigma}}U = I + B'$ in Eq. (22) has the desired form of Eq. (19), with B' only containing diagonal elements. Now the standard CPQMC algorithm can be applied using the new formula of Eq. (22). A similar modification can also be applied to the matrix inverse $(\langle\phi'|e^{\lambda\alpha f_{i\sigma}}|\phi\rangle)^{-1}$.

[1] D. C. Johnston, Adv. Phys. **59**, 803 (2010).
[2] P. J. Hirschfeld, M. M. Korshunov, and I. I. Mazin, Rep. Prog. Phys. **74**, 124508 (2011).
[3] E. Dagotto, Rev. Mod. Phys. **85**, 849 (2013).
[4] P. Dai, J. P. Hu, and E. Dagotto, Nat. Phys. **8**, 709 (2012).
[5] N. Mannella, J. Phys.: Condens. Matter **26** 473202 (2014).
[6] Elena Bascones, Belén Valenzuela, and Maria José Calderón, Comptes Rendus Physique **17**, 36 (2016).
[7] Julián Rincón, Adriana Moreo, Gonzalo Alvarez, and Elbio Dagotto, Phys. Rev. Lett. **112**, 106405 (2014).
[8] Julián Rincón, Adriana Moreo, Gonzalo Alvarez, and Elbio Dagotto, Phys. Rev. B **90**, 241105(R) (2014).
[9] V. I. Anisimov, I. A. Nekrasov, D. E. Kondakov, T. M. Rice, and M. Sigrist, Eur. Phys. J. B **25**, 191 (2002).
[10] A. Georges, L. dé Medici, and J. Mravlje, Annu. Rev. Condens. Matter Phys. **4**, 137 (2013).
[11] M. Yi, Z-K Liu, Y. Zhang, R. Yu, J.-X. Zhu, J.J. Lee, R.G. Moore, F.T. Schmitt, W. Li, S.C. Riggs, J.-H. Chu, B. Lv, J. Hu, M. Hashimoto, S.-K. Mo, Z. Hussain, Z.Q. Mao, C.W. Chu, I.R. Fisher, Q. Si, Z.-X. Shen and D.H. Lu, Nat. Commun. **6**, 7777(2015).
[12] M. Yi, D. H. Lu, R. Yu, S. C. Riggs, J.-H. Chu, B. Lv, Z. K. Liu, M. Lu, Y.-T. Cui, M. Hashimoto, S.-K. Mo, Z. Hussain, C. W. Chu, I. R. Fisher, Q. Si, and Z.-X. Shen, Phys. Rev. Lett. **110**, 067003 (2013).
[13] A. Liebsch, Phys. Rev. B **70**, 165103 (2004).
[14] S. Biermann, L. dé Medici, and A. Georges, Phys. Rev. Lett. **95**, 206401 (2005).
[15] L. dé Medici, S. R. Hassan, M. Capone, and X. Dai, Phys. Rev. Lett. **102**, 126401 (2009).
[16] H. Ishida and A. Liebsch, Phys. Rev. B **81**, 054513 (2010).
[17] L. dé Medici, J. Mravlje, and A. Georges, Phys. Rev. Lett. **107**, 256401 (2011).
[18] E. Bascones, B. Valenzuela, and M. J. Calderón, Phys. Rev. B **86**, 174508 (2012).
[19] M. Greger, M. Kollar, and D. Vollhardt, Phys. Rev. Lett. **110**, 046403 (2013).
[20] K. Haule and G. Kotliar, New J. Phys. **11**, 025021 (2009).
[21] Q. Luo, G. Martins, D.-X. Yao, M. Daghofer, R. Yu, A. Moreo, and E. Dagotto, Phys. Rev. B **82**, 104508 (2010).
[22] Z. P. Yin, K. Haule, and G. Kotliar, Nat. Mater. **10**, 932 (2011).
[23] J. Ferber, K. Foyevtsova, R. Valentí, and H. O. Jeschke, Phys. Rev. B **85**, 094505 (2012).
[24] Richard T. Scalettar, Reinhard M. Noack, and Rajiv R. P. Singh Phys. Rev. B **44**, 10502 (1991)
[25] S. Liang, A. Moreo, and E. Dagotto, Phys. Rev. Lett. **111**, 047004 (2013).
[26] S. Liang, A. Mukherjee, N. D. Patel, C. B. Bishop, E. Dagotto, and A. Moreo, Phys. Rev. B **90**, 184507 (2014).
[27] J. M. Caron, J. R. Neilson, D. C. Miller, A. Llobet, and T. M. McQueen, Phys. Rev. B **84**, 180409(R) (2011).
[28] J. M. Caron, J. R. Neilson, D. C. Miller, K. Arpino, A. Llobet, and T. M. McQueen, Phys. Rev. B **85**, 180405(R) (2012)
[29] Q. Luo, A. Nicholson, J. Rincón, S. Liang, J. Riera, G. Alvarez, L. Wang, W. Ku, G. D. Samolyuk, A. Moreo, and E. Dagotto, Phys. Rev. B **87**, 024404 (2013).
[30] Q. Luo and E. Dagotto, Phys. Rev. B **89**, 045115 (2014), and references therein.
[31] Q. Luo, A. Nicholson, J. Riera, D.-X. Yao, A. Moreo, and E. Dagotto, Phys. Rev. B **84**, 140506 (2011), and references therein.
[32] Q. Luo, K. Foyevtsova, G. D. Samolyuk, F. Reboredo, and E. Dagotto, Phys. Rev. B **90**, 035128 (2014).
[33] E. Dagotto, T. Hotta, and A. Moreo, Phys. Rep. **344**, 1 (2001).
[34] S. R. White, Phys. Rev. Lett. **69**, 2863 (1992).
[35] U. Schollwöck, Rev. Mod. Phys. 77, 259 (2005).
[36] K. Hallberg, Adv. Phys. **55**, 477 (2006).
[37] R. Blankenbecler, D. J. Scalapino, and R. L. Sugar, Phys. Rev. D **24**, 2278 (1981).
[38] S. R. White, D. J. Scalapino, R. L. Sugar, E. Y. Loh, J. E. Gubernatis, and R. T. Scalettar, Phys. Rev. B **40**, 506 (1989).
[39] D. M. Ceperley and M. H. Kalos, *Chapter 4, Quantum Many-body Problems*, Monte Carlo Methods in Statistical Physics (Springer-Verlag Berlin Heidelberg 1986).
[40] S. Zhang, J. Carlson, and J. E. Gubernatis, Phys. Rev. B **55**, 7464 (1997).
[41] S. Zhang, J. Carlson, and J. E. Gubernatis, Phys. Rev. Lett. **78**, 4486 (1997).
[42] Guangkun Liu, Zhongbing Huang, Yongjun Wang, J. Phys.: Condens. Matter, **26** 325601 (2014)
[43] J. Carlson, J. E. Gubernatis, G. Ortiz, and Shiwei Zhang Phys. Rev. B **59**, 12788 (1999).
[44] For a recent reference on DQMC see V. I. Iglovikov, E. Khatami, and R. T. Scalettar, Phys. Rev. B **92**, 045110 (2015).
[45] E. Y. Loh, Jr., J. E. Gubernatis, R. T. Scalettar, S. R. White, D. J. Scalapino, and R. L. Sugar, Phys. Rev. B **41**, 9301 (1990).
[46] Some recently proposed techniques for multiorbital Hubbard models combine mean-field approximations with classical Monte Carlo approaches. See Anamitra Mukherjee, Niravkumar D. Patel, Shuai Dong, Steve Johnston, Adriana Moreo, and Elbio Dagotto, Phys. Rev. B **90**, 205133 (2014); Anamitra Mukherjee, Niravkumar D. Patel, Adriana Moreo, and Elbio Dagotto, Phys. Rev. B **93**, 085144 (2016)
[47] M. Guerrero, J. E. Gubernatis, and Shiwei Zhang, Phys.

Rev. B **57**, 11980 (1998).
[48] J. Bonča, J. E. Gubernatis, M. Guerrero, Eric Jeckelmann, and Steven R. White, Phys. Rev. B **61**, 3251 (2000).
[49] Z. B. Huang, H. Q. Lin, and E. Arrigoni, Phys. Rev. B **83**, 064521 (2011).
[50] Tianxing Ma, Zhongbing Huang, Feiming Hu, and Hai-Qing Lin, Phys. Rev. B **84**, 121410(R) (2011).
[51] Chia-Chen Chang and Shiwei Zhang, Phys. Rev. B **78**, 165101 (2008)
[52] The free-electron wave function was also tried as a trial wave function in our simulations. However, except in the very weak coupling regime, the free-electron wave function always induced a higher CPQMC energy.
[53] J. E. Hirsch, Phys. Rev. B **28**, 4059 (1983)
[54] S. Sakai, R. Arita and H. Aoki, Phys. Rev. B **70**, 172504 (2004)
[55] W. Gropp, E. Lusk, N. Doss, and A. Skjellum, Parallel Computing **22**, 789, (1996).
[56] See *www.open-mpi.org*.
[57] C.-C. Chang, S. Gogolenko, J. Perez, Z. Bai, and R. T. Scalettar, Philos. Mag. B **95**, 1260 (2013).
[58] K. Bouadim, G. G. Batrouni, F. Hébert, and R. T. Scalettar, Phys. Rev. B **77**, 144527 (2008).
[59] L. Rademaker, S. Johnston, J. Zaanen, and J. van den Brink, Phys. Rev. B **88**, 235115 (2013).
[60] K. Held and D. Vollhardt, Eur. Phys. J. B **5**, 473 (1998).
[61] Y. Motome and M. Imada, J. Phys. Soc. Jpn. **66**, 1872 (1997).
[62] T. Hotta, M. Moraghebi, A. Feiguin, A. Moreo, S. Yunoki, and E. Dagotto, Phys. Rev. Lett. **90**, 247203 (2003).
[63] T. Hotta, S. Yunoki, M. Mayr, and E. Dagotto, Phys. Rev. B **60**, 15009 (1999).
[64] S. Dong, R. Yu, S. Yunoki, J.-M. Liu, and E. Dagotto. Phys. Rev. B **78**, 155121 (2008).
[65] E. Dagotto, J. Burgy and A. Moreo, Solid State Communications **126**, 9 (2003).